Chemical Science

Accepted Manuscript

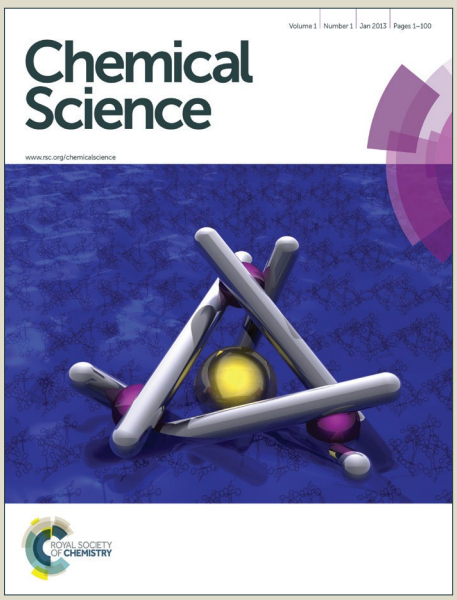

ROYAL SOCIETY OF CHEMISTRY

www.rsc.org/chemicalscience

Chemical Science

ARTICLE

Radical Transfer in *E. coli* Ribonucleotide Reductase: A $NH_2Y_{731}/R_{411}A$-α mutant unmasks a new conformation of the pathway residue 731.

Received 00th January 20xx,
Accepted 00th January 20xx

DOI: 10.1039/x0xx00000x

www.rsc.org/

Müge Kasanmascheff,[a, b, ‡] Wankyu Lee,[c, ‡] Thomas U. Nick,[a] JoAnne Stubbe,[c,*] Marina Bennati [a, b, *]

Ribonucleotide reductases (RNRs) catalyze the conversion of ribonucleotides to deoxyribonucleotides in all living organisms. The catalytic cycle of *E. coli* RNR involves a long-range proton-coupled electron transfer (PCET) from a tyrosyl radical (Y_{122}•) in subunit β2 to a cysteine (C_{439}) in the active site of subunit α2, which subsequently initiates nucleotide reduction. This oxidation occurs over 35 Å and involves a specific pathway of redox active amino acids (Y_{122} ↔ [W_{48}?] ↔ Y_{356} in β2 to Y_{731} ↔ Y_{730} ↔ C_{439} in α2). The mechanisms of PCET steps at the interface of the $\alpha2\beta2$ complex remain puzzling due to lack of structural information in this region. Recently, DFT calculations on the 3-aminotyrosyl radical (NH_2Y_{731}•)-α2 trapped by incubation of NH_2Y_{731}-$\alpha2/\beta2$/CDP(substrate)/ATP(allosteric effector), suggested that R_{411}-α2, a residue close to the $\alpha2\beta2$ interface, interacts with NH_2Y_{731}• and accounts in part for its perturbed EPR parameters. To examine its role, we have further modified NH_2Y_{731}-α2 with a R_{411}A substitution. NH_2Y_{731}•/R_{411}A generated upon incubation of NH_2Y_{731}/R_{411}A-$\alpha2/\beta2$/CDP/ATP was investigated using multi-frequency (34, 94 and 263 GHz) EPR, 34 GHz pulsed electron-electron double resonance (PELDOR) and electron-nuclear double resonance (ENDOR) spectroscopies. The data indicate a large conformational change of NH_2Y_{731}•/R_{411}A relative to the NH_2Y_{731}• single mutant. Particularly, the inter spin distance of NH_2Y_{731}•/R_{411}A in one $\alpha\beta$ pair to Y_{122}• in the second $\alpha\beta$ pair decreases by 3 Å in the presence of R_{411}A mutation. This is the first experimental evidence for the flexibility of pathway residue Y_{731}-α2 in an $\alpha2\beta2$ complex and suggests a role for R_{411} in the stacked Y_{731}/Y_{730} conformation involved in collinear PCET. Furthermore, NH_2Y_{731}•/R_{411}A serves as a probe of the PCET process across the subunit interface.

Introduction

Coupling of electron and proton transfers between donors and acceptors in proteins are ubiquitous in biology and can occur in a stepwise or concerted fashion. The concerted case avoids high energy intermediates and is designated proton coupled electron transfer (PCET).[1] The mechanisms of these couplings are fundamental to our understanding of photosynthesis, respiration, synthesis of DNA building blocks, and many additional processes. Unresolved issues describing these mechanisms have been articulated in several recent comprehensive reviews with different mechanisms dictated by transfer distances, protein environment and dynamics.[2, 3] When the proton and electron donor to the acceptor are distinct, the mechanism involves orthogonal PCET; when the donor and acceptor are the same, it involves collinear PCET.[4, 5] A different mechanism in which a proton is transferred through water chains over long distances in concert with electron transfer (ET) has also recently been studied and discussed extensively in model systems.[6, 7] In all mechanistic cases, since the electrons and protons have very different masses, electrons tunnel over large distances (10-15 Å) while proton tunnelling is restricted to shorter distances, on the order of H-bond lengths.[1, 8, 9] This distance dependence complicates the issue of proton management. One important representative of the diversity of PCET mechanisms in proteins is found in the class I ribonucleotide reductases (RNRs). These enzymes catalyze the conversion of nucleotides to deoxynucleotides, the monomeric precursors required for DNA replication and repair in all eukaryotic and some prokaryotic organisms.[10, 11] In this paper we use the *Escherichia coli* (*E. coli*) class Ia RNR as a model system, to interrogate the PCET process across the interface of the two subunits of this enzyme, proposed to involve two redox active protein tyrosine residues, one on each subunit, and a water interface between the subunits.[12]

The *E. coli* RNR consists of two homodimeric subunits, α2 and β2.[13] The enzyme is active when a transient $\alpha2\beta2$ complex is formed.[14] α2 contains the active site for nucleotide reduction and two allosteric effector binding sites that regulate the specificity and the rate of reduction.[15-19] β2 harbors the essential di-iron tyrosyl radical cofactor (Fe^{III}_2-Y_{122}•).[20, 21] During each turnover Y_{122}•-β oxidizes C_{439}-α to a thiyl radical, which subsequently initiates dNDP production.[11] There are X-ray structures of the individual subunits

[a] *Max Planck Institute for Biophysical Chemistry, 37077 Göttingen, Germany, E-mail: marina.bennati@mpibpc.mpg.de*
[b] *Department of Chemistry, University of Göttingen, 37077 Göttingen, Germany*
[c] *Department of Chemistry, Massachusetts Institute of Technology, Cambridge, Massachusetts 02139, United States, E-mail: stubbe@mit.edu*
Electronic Supplementary Information (ESI) available: See DOI: 10.1039/x0xx00000x

‡ These authors contributed equally.

and a docking model of the $\alpha 2\beta 2$ complex places Y_{122}• at a distance of about 35 Å from C_{439}.[22, 23] These initial studies led to the first formulation of radical transfer (RT) in RNR via a radical hopping mechanism involving a pathway of conserved amino acids (Y_{122} ↔ [W_{48}?] ↔ Y_{356} in β to Y_{731} ↔ Y_{730} ↔ C_{439} in α). Biochemical[24] and biophysical (EPR[25, 26], SAXS[27], cryoEM[28]) studies confirmed that the docking model provides a reasonable representation of *E. coli* RNR in its transient, active form and led to a detailed mechanism of RT over such a long distance.[4, 14, 24] Nevertheless, in wild-type (wt) *E. coli* RNR, the rate limiting step, conformational change(s) upon substrate and allosteric effector binding to $\alpha 2$, has prevented spectroscopic detection of any intermediates in this process.[29] The recent development of methods to site-specifically incorporate tyrosine analogs with altered pK_as and reduction potentials has permitted detection of pathway radical intermediates[30-32] and combined with state-of-the-art EPR spectroscopy[12, 26, 33, 34] has started to reveal the molecular basis of the long-range RT in RNR.[14] These experiments have led to the current model illustrated in Figure 1, which involves orthogonal PCET[35] steps within subunit $\beta 2$ and collinear PCET steps within the $\alpha 2$ subunit.[12, 33] However, the mechanism of the PCET process at the subunit interface between Y_{356} in $\beta 2$ and Y_{731} in $\alpha 2$ remains elusive as structural information on the C-terminal 35 amino acids of $\beta 2$, including a putative proton acceptor E_{350} and Y_{356} (Fig. 1) is missing.[22]

Our recent high-field (HF) EPR/ENDOR and DFT investigations using the 3-amino tyrosine mutants NH_2Y_{730}-$\alpha 2$ and NH_2Y_{731}-$\alpha 2$, which generate the corresponding NH_2Y• upon incubation with $\beta 2$, CDP (substrate) and ATP (allosteric effector), established that an unusual stacked conformation of residues 730 and 731, observed in some X-ray structures of $\alpha 2$[23, 36] (see Supporting Information, Figure S1), occurs in the $\alpha 2\beta 2$ complex.[12, 33] However, the X-ray structure of NH_2Y_{730}-$\alpha 2$ (PDB 2XO4) alone reported multiple conformations for Y_{731}-$\alpha 2$, with one rotated away from NH_2Y_{730}-$\alpha 2$ toward the $\alpha 2\beta 2$ subunit interface.[30] This "flipped" conformation was accompanied by reorientations of R_{411} and N_{733} in $\alpha 2$. Further comparison of NH_2Y_{730}•-α, NH_2Y_{731}•-α and NH_2Y_{356}•-β by HF-EPR indicated that the electrostatic environment of all three transient NH_2Y•s is strongly perturbed and their hydrogen bond interactions are intrinsically different.[12, 33] Interestingly, one of our DFT models of the protein environment for NH_2Y_{731}•-$\alpha 2$ required R_{411}-$\alpha 2$ to recapitulate the perturbed g_x value observed and suggested that it approaches NH_2Y_{731}•-$\alpha 2$ within 2.6 Å (Figure S1).[12] Therefore, to examine the role of R_{411}-$\alpha 2$ during the PCET process in *E. coli* RNR, we generated two mutants: R_{411}A-$\alpha 2$ and the double mutant NH_2Y_{731}/R_{411}A-$\alpha 2$. Here, we report the incubation of NH_2Y_{731}/R_{411}A-$\alpha 2$ with $\beta 2$/CDP and ATP that generates the NH_2Y_{731}•/R_{411}A-$\alpha 2\beta 2$ complex. Using advanced EPR methods, including 263 GHz pulse EPR and 34 GHz PELDOR/DEER (pulsed electron-electron double resonance) and ENDOR (electron-nuclear double resonance) spectroscopies, we have provided evidence for a new conformation of NH_2Y_{731}•-$\alpha 2$ that is "flipped" towards the subunit interface in the $\alpha 2\beta 2$ complex. This is the first time an alternative conformation of any pathway tyrosine (NH_2Y_{731}•) has been observed and it provides a new probe of the PCET mechanism across the subunit interface that remains unknown.

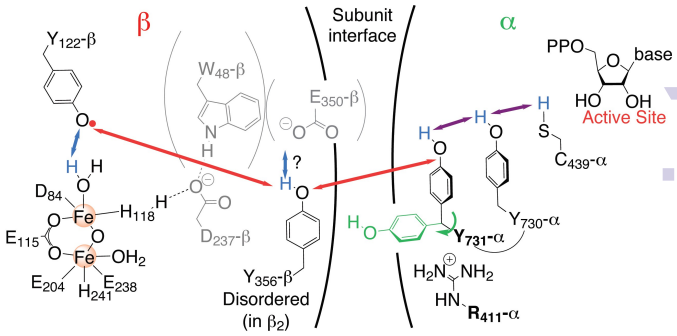

Figure 1. Current model of the long-range PCET in *E. coli* RNR. R_{411} is shown along with the redox active amino acid residues that are involved in this process (Y_{122} ↔ [W_{48}?] ↔ Y_{356} in $\beta 2$ ↔ Y_{731} ↔ Y_{730} ↔ C_{439} in $\alpha 2$). W_{48}, D_{237} and E_{350} are shown in grey, because currently there is no evidence for their role in this process.[14] The location of Y_{356} and E_{350} are unknown as they are within the flexible C-terminal tail (35 amino acids) of $\beta 2$. Red, blue and purple arrows represent electron transfer, proton transfer and colinear PCET pathways, respectively.

Experimental

Materials. 4-(2-Hydroxyethyl)-1-piperazineethanesulfonic acid (Hepes) was purchased from EMD Bioscience. Adenosine-5'-triphosphate (ATP), cytidine-5'-diphosphate (CDP), reduced β-nicotinamide adenine dinucleotide phosphate (NADPH), hydroxyurea (HU), kanamycin (Km), chloramphenicol (Cm), 2XYT media, M9 Minimal Salts, L-arabinose (ara), β-mercaptoethanol (β-ME), streptomycin sulfate and NH_2Y were purchased from Sigma-Aldrich. Isopropyl-β-D-thiogalactopyranoside (IPTG) and 1,4-dithiothreitol (DTT) were purchased from Promega. Tris (2-carboxyethyl) phosphine (TCEP) hydrochloride was purchased from Thermo Scientific. Nucleotide primers were purchased from Invitrogen and Pfu Ultra II polymerase was purchased from Stratagene.

Site-directed mutagenesis to generate R_{411}A-$\alpha 2$ and NH_2Y_{731}/R_{411}A-$\alpha 2$. The Quikchange kit (Stratagene) was used according to manufacturer's protocol to generate each mutant. The templates pET28a-nrdA or pET28a-nrdA $Y_{731}Z$[30] were amplified with primer 5`-G CAG GAA CGT GCG TCT ACC GGT GCG ATC TAT ATT CAG AAC GTT GAC-3` and its reverse complement and used to insert a GCG (Ala) at position 411. The sequences were confirmed by QuintaraBio Laboratory. All constructs contain an N-terminal $(His)_6$-tag with a 10 amino acid linker.[30]

Expression, purification and activity assays of R_{411}A-$\alpha 2$ and NH_2Y_{731}/R_{411}A-$\alpha 2$. $(His)_6$-wt-$\alpha 2$ (2750 nmol/min/mg) and wt-$\beta 2$ (7000 nmol/min/mg, 1.2 Y•/$\beta 2$ were expressed and purified by standard protocols.[30, 37, 38] All $\alpha 2$ mutants were pre-reduced with 30 mM DTT and 15 mM HU before use.[29] *E. coli* thioredoxin (TR, 40 U/mg) and thioredoxin reductase (TRR, 1800 U/mg) used in assays were isolated as previously described.[39, 40] $(His)_6$-NH_2Y_{731}-$\alpha 2$ was purified as previously described.[30] Expression and purification of R_{411}A-$\alpha 2$ and NH_2Y_{731}/R_{411}A-$\alpha 2$ followed previous protocols[30] except that the purification buffer (50 mM Tris, 5% glycerol, 1 mM PMSF, pH 7.6) for NH_2Y_{731}/R_{411}A-$\alpha 2$ contained 1 mM TCEP. The yield of purified R_{411}A-$\alpha 2$ and NH_2Y_{731}/R_{411}A-$\alpha 2$ was 10-12 mg/g and 6-7 mg/g cell paste, respectively. The activity of R_{411}A-$\alpha 2$ (0.2 μM) and NH_2Y_{731}/R_{411}A-$\alpha 2$ (1 μM) was determined in the

presence of 50-fold excess of wt-β2 with 3 mM ATP, 1 mM [^{3}H]-CDP (4850 cpm/nmol), 30 μM TR, 0.5 μM TRR, 1 mM NADPH in assay buffer (50 mM HEPES, 1 mM EDTA, 15 mM $MgSO_4$ pH 7.6). The amount of dCDP was determined by the method of Steeper and Steuart.[41] For single turnover experiments, NH_2Y_{731}/R_{411}A-α2 (5 μM) was incubated with wt-β2 (5 μM), 3 mM ATP, 1 mM [^{3}H]-CDP (20,000 cpm/nmol) in assay buffer. The dissociation constant (K_d) for R_{411}A-α2 and wt-β2 was determined in H_2O and D_2O buffers by the competitive inhibition assay[42] (SI-2, Fig. S2).

Samples for HF EPR and PELDOR spectroscopy. NH_2Y_{731}/R_{411}A-α2 and wt-β2 were mixed 1:1 to a final concentration of 160 – 180 μM in D_2O assay buffer as previously described.[32, 34] These protein concentrations resulted in >95% binding between subunits. The reaction was initiated at room temperature by adding CDP and ATP to a final concentration of 1 and 3 mM, respectively. The reactions were manually freeze-quenched in liquid N_2 within 10 –23 s. The PELDOR sample was prepared by adding glycerol-$(OD)_3$ 16 s after the initiation of the reaction to a final concentration of 10% (v:v). This reaction was manually freeze-quenched after 56 s as just described. The NH_2Y_{731}• accounted for 30–33% of the total spin for all the samples used in this work and was similar to the yields reported previously.[30, 32]

HF-pulsed EPR spectroscopy. Echo-detected (ESE: $\pi/2 - \tau - \pi -$ echo) EPR spectra at 263 GHz were recorded on a Bruker Elexsys E780 quasi optical spectrometer using a single mode (TE_{011}) cylindrical resonator (E9501610 – Bruker BioSpin) with a typical quality factor of 500 – 1000. Maximum microwave power coupled to the resonator was about 15 mW. Samples for 263 GHz EPR were inserted in capillaries (0.33 OD, Vitrocom CV2033S) in typical volumes of ca. 50 nL. 94 GHz ESE spectra were recorded on a Bruker E680 spectrometer with 400 mW W-band power setup (Bruker power upgrade – 2). Samples for 94 GHz contained typical volumes of 2 μL in 0.84 OD capillaries (Wilmad S6X84). All manually freeze quenched samples immersed in liquid N_2 were loaded into precooled EPR cryostats.

34 GHz PELDOR spectroscopy. 34 GHz ESE and PELDOR spectra were recorded on a Bruker E580 X/Q-band spectrometer equipped with a Bruker EN 5107D2 pulse EPR/ENDOR resonator. The spectrometer was power-upgraded with a Q-band TWT amplifier providing about 170 W output power at 34.1 GHz. PELDOR experiments were recorded with an overcoupled resonator. The center of the mode was chosen for the pump frequencies for measurements at 20 K. However, for measurements at 50 K the detection frequency was set in the center of the cavity mode to enhance detection sensitivity. Q-band samples contained typical volumes of 10 μL in 1.6 mm OD capillaries (Wilmad 222T-RB).

Processing and simulation of EPR spectra. Spectra were processed by phasing and baseline correction. Derivatives of the absorption spectra were obtained by fitting every four points with a second order polynomial and differentiating the function in MATLAB_R2014b.[43] EPR spectra were simulated using EasySpin-4.5.5 "pepper"-routine running under MATLAB.[44]

DFT calculations. DFT calculations have been performed with the ORCA 3.0.0 program package.[45] The geometry optimization of the neutral NH_2Y• was performed on the unrestricted B3LYP[46-48] hybrid density functional in combination with the def2-TZVPP basis set and def2-TZVPP/JK auxiliary basis set.[49, 50] To take into account the electrostatic environment of the radical intermediate at the protein interface a solvation model (COSMO[51]) with the polarity of ethanol (ε=24) was used. Otherwise Grimme's dispersion correction[52, 53] and RIJCOSX[54] approximations have been employed. The energy converged to 10^{-9} E_h. The hyperfine couplings and *g*-values were calculated using the NH_2Y• C_4 as gauge origin.[55, 56] The def2-TZVPP basis set was held consistent with the geometry optimization step.[50] The C2-C1-Cβ-Cα dihedral angle of the NH_2Y• was changed stepwise with a geometry optimization for each step. One of the optimized models in *xyz* coordinates is given in Supporting Information.

PyMOL models. The docking model refers to the $\alpha2\beta2$ complex structure generated from the individual wt-α2 and wt-β2 X-ray structures.[22, 23] In order to predict distances, the mutant *E. coli* RNR structure (PDB 2XO4)[30] was overlaid with the wt-α2 structure in the docking model[23] using PyMOL, which first performs a sequence alignment and then aligns the structures to minimize the root mean square deviation between the structures.

Results and discussion

Preparation and characterization of R_{411}A-α2, NH_2Y_{731}/R_{411}A-α2 and ND_2Y_{731}•/R_{411}A-α. Our recent studies on NH_2Y_{731}-α2[12] suggested that R_{411} might interact with NH_2Y_{731}•, partially accounting for the measured EPR and ENDOR parameters. To investigate this proposal, R_{411}A-α2 was generated and characterized. Because the mutation is proposed to be at the interface of α2 and β2, the dissociation constant (K_d) for subunit interactions was also examined and determined to be 0.94 ± 0.33 μM (Fig. S2A), ~5 fold higher than that for wt-α2 (0.18 μM).[42] Under these conditions, this mutant was shown to have a specific activity of 467 ± 22 nmol/min/mg, 17% that of the wt enzyme (2750 nmol/min/mg). The reduced activity and weaker subunit binding suggests that R_{411} plays a role in function.

Furthermore, we characterized the role of R_{411} in the oxidation of Y_{731}-α2 by generating the double mutant NH_2Y_{731}/R_{411}A-α2. The K_d for subunit interactions between NH_2Y_{731}/R_{411}A-α2 and wt-β2 was determined to be 8 ± 1 nM (Fig. S2C), which is consistent with formation of a tight complex when a NH_2Y• is generated.[28] Its specific activity was 13 ± 3 nmol/min mg, 0.4% of wt-RNR and in the range of contaminating wt-α2 activity.[32] A more sensitive, one turnover assay was then employed to determine if this double mutant could generate any dCDP. When pre-reduced NH_2Y_{731}/R_{411}A-α2 was mixed with wt-β2, CDP, ATP for 5 min, only 0.036 ± 0.018 dCDP/α2 were observed, consistent with contaminating wt-α2. Thus the double mutant is unable to make detectable dCDP, not unexpected, given the specific activity of the R_{411}A and the NH_2Y_{731}-α2 mutants (see also SI-3 and Fig. S3).

We next investigated whether NH_2Y_{731}• could be generated with NH_2Y_{731}/R_{411}-α2, despite its inability to make dCDPs. NH_2Y_{731}/R_{411}A-α2, wt-β2, CDP and ATP were studied by stopped-flow (SF) spectroscopy and the reaction was monitored at 320 nm, the absorption feature associated with the NH_2Y• (Fig. S4, red). The data were fit in two time domains: 5 ms to 6 s and 25 s to 100 s. In the first time domain, NH_2Y_{731}• formation was fit to a double exponential with k_{fast} of 3.6 ± 0.5 s^{-1} (amplitude 8%) and k_{slow} of 0.47 ± 0.03 s^{-1} (amplitude 21%) (Table S1). The rate constants for

NH_2Y_{731}• in the single mutant control were similar: k_{fast} of 9.6 ± 0.6 s^{-1} and a k_{slow} of 0.8 ± 0.1 s^{-1}. However, in this case, the fast phase accounted for 27% and the slow phase 13% of the NH_2Y_{731}•. The biphasic kinetics of NH_2Y_{731}• formation in both cases is attributed to multiple conformations giving rise to NH_2Y_{731}•.[32] From 25 s to 100 s, NH_2Y_{731}• in the double mutant reaction disappeared with a k_{obs} of 0.02 ± 0.003 s^{-1} while with the single mutant, disappearance occurred with a k_{obs} of 0.005 ± 0.002 s^{-1}. Analysis of the Y_{122}•-β disappearance kinetics was unsuccessful at early time points due to the detection limits, as described in SI-4.

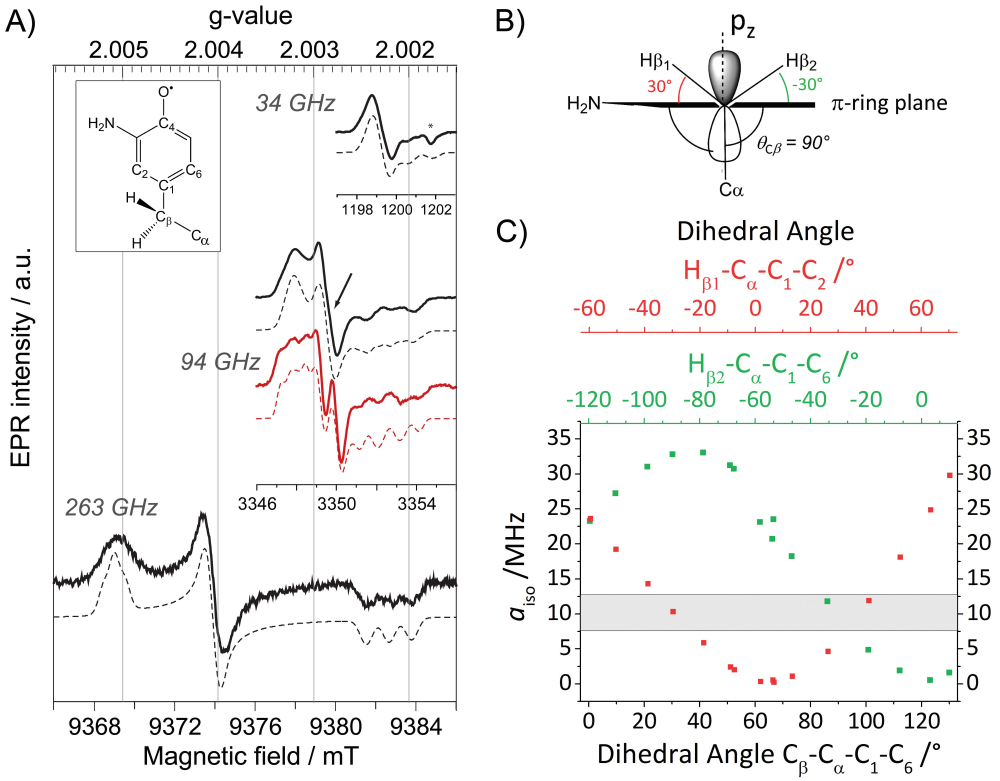

Figure 2. A) Derivative EPR spectra (solid black lines) at 34 GHz (top), 94 GHz (middle) and 263 GHz (bottom) of ND_2Y_{731}•/R_{411}A-α2 with corresponding simulations (dashed black lines). 94 GHz EPR spectrum of ND_2Y_{731}•-α2 in the single mutant (solid red line) with corresponding simulation (dashed red line) is shown for comparison. The difference between two spectra around g_y is marked with an arrow. A glass signal is marked with an asterisk. Exp. conditions (34 GHz): $\pi/2$ = 6 ns, τ = 280 ns, shot repetition time = 6 ms, shots/point = 80, number of scans = 10; (94 GHz): $\pi/2$ = 30 ns, τ = 280 ns, shot repetition time = 5 ms, shots/point = 100, number of scans = 50 – 100; (263 GHz): $\pi/2$ = 40 ns, τ = 270 ns, shot repetition time = 6 ms, shots/point = 250, number of scans = 36. Structure of a NH_2Y is shown in the inset. **B**) Orientation of the Cβ-methylene protons with respect to phenol ring as extracted from the observed hyperfine couplings. **C)** a_{iso} as a function of the dihedral angle for each Cβ-methylene protons calculated from a DFT model for NH_2Y• (Figure S6).

Given the distinct kinetics of our double mutant relative to the NH_2Y_{731}-α2, the 9 GHz EPR spectrum of the sample generated from the reaction of NH_2Y_{731}/R_{411}A-α2 with wt-β2, ATP, CDP and quenched at 25 s was recorded and is shown in Figure S5A and S5C. Subsequent to subtraction of Y_{122}•, 32% of the total spin is associated with NH_2Y_{731}•/R_{411}A-α2 with no spin loss. This result is similar to that of the single mutant, NH_2Y_{731}•.[30, 32] A comparison of their spectra shown in Figure S5B revealed substantial differences in their hyperfine interactions, suggesting that further characterization of this radical might provide insight about the function of R_{411}. Therefore, the role of R_{411} in the RT pathway was further studied with advanced EPR spectroscopy.

HF EPR of ND_2Y_{731}•/R_{411}A-α2. To examine the generated ND_2Y_{731}•/R_{411}A-α2, we took advantage of the proximity of Y_{122}• to the diiron cluster and its altered relaxation properties. Pulsed EPR spectra at 34, 94 and 263 GHz of ND_2Y_{731}•/R_{411}A-α2 were recorded in D_2O buffer at 70 K and are shown in Figure 2. The use of D_2O considerably simplifies the EPR spectra due to the absence of ^{1}H hyperfine (hf) splittings from the amino protons. The ND_2Y_{731}•/R_{411}A-α2 EPR spectrum at 34 GHz is mainly dominated by the large hf couplings from the deuterons of the amino group and the two Cβ-methylene protons.[34] On the other hand, 94 and 263 GHz EPR spectra are dominated by g-anisotropy, with relative contribution of g- and hf-anisotropy strongly dependent on the operating magnetic field. The g-values of ND_2Y_{731}•/R_{411}A-α2 are best resolved at 263 GHz and are consistent with the values from our previous ND_2Y• studies.[12, 33] The 94 GHz spectrum reveals the differences in the hf splitting of the Cβ-methylene protons (Fig. 2A, marked with an arrow): the large hf splitting of the Cβ-methylene proton visible in the central line of ND_2Y_{731}•-α2 (red), is now missing in ND_2Y_{731}•/R_{411}A-α2 (black). This splitting is absent also in the 263 GHz spectrum. The EPR spectra were simulated iteratively to find a global solution for the contributing hf couplings. All of the EPR data and simulations, in which the previously reported[34] hf coupling for ^{14}N is used, are consistent with NH_2Y_{731}• generated in the NH_2Y_{731}•/R_{411}A-α2/β2 complex being a single, well-oriented radical species with one set of magnetic parameters listed in Table 1 (see also Fig. S7). This finding is not self-evident as our previous

experiments with other double mutants NH_2Y_{731}•/Y_{730}F-$\alpha 2$ and NH_2Y_{730}•/C_{439}A-$\alpha 2$ showed distributions in *g*-values indicative of multiple radical environments and/or molecular orientations.[12]

Table 1. Summary of *g*-values and large hf couplings (> 8 MHz) of ND_2Y_{731}• in the double and single mutants.

Samples	*g*-values			a_{iso} (MHz)		
	g_x	g_y	g_z	Hβ_1	Hβ_2	^{14}N
ND_2Y_{731}•/R_{411}A-α	2.0051	2.0041	2.0022	10	10	12
ND_2Y_{731}•-α [a]	2.0051	2.0041	2.0022	22	9	12

Uncertainty in the *g*-values and hf couplings are about 0.00005 and up to 10% from spectral simulations, respectively. a) *g*-values and hf couplings were reported in Ref. 12 and Ref. 34 respectively.

Interestingly, we do not observe changes in *g*-values between ND_2Y_{731}•/R_{411}A-α and ND_2Y_{731}•-$\alpha 2$. This is unexpected because the g_x value is the reporter of the electrostatic environment of a radical,[57] and the R_{411}A mutation has changed the local environment of ND_2Y_{731}•, demonstrated by the substantial change in the Cβ-methylene ^{1}H couplings (Table 1). These couplings are related to the dihedral angle $\theta_{C\beta}$ between the Cβ-H bond and the p_z orbital axis of C_1 (Fig. 2B) and therefore, provide information on the molecular orientation of tyrosyl and 3-aminotyrosyl radicals.[34] The dihedral angle can be extracted from the McConnell equation ($a_{iso(C^{\beta}\text{-}H)} = B_1 \cdot \rho_{C1} \cdot \cos^2\theta_{C\beta}$),[58] which provides a semi empirical relationship for the observed isotropic constant a_{iso}. The angle C2-C1-Cβ-Cα of ND_2Y_{731}•/R_{411}A-$\alpha 2$ is estimated to be ≈ 90° by using B_1 of 162 MHz[59] for tyrosyl radicals, an electron spin density ρ_{C1} of 0.214[12], and an isotropic Cβ-methylene proton hf coupling a_{iso} = 10 ± 1 MHz (Table 1). This dihedral angle indeed is consistent with the hf couplings of the two Cβ-methylene ^{1}H resonances being indistinguishable, as reported in Table 1 and seen in Figures 2B and C. The result was confirmed by a DFT calculation on the NH_2Y• for the observed hf couplings where the ring orientation was modeled with respect to the backbone and shows a symmetric orientation relative to the p_z orbital axis of C_1, Figure 2B. In this calculation $\theta_{C\beta}$ angle of 90° corresponds to a_{iso} = 9 ± 3 MHz (grey area in Figure 2C) for both Cβ-methylene protons $H_{\beta 2/1}$.

ENDOR for detection of hydrogen bonds to ND_2Y_{731}•/R_{411}A-$\alpha 2$. Given that the R_{411}A mutation had little effect on g_x, ^{2}H ENDOR spectroscopy was used to further examine a possible correlation of the observed g_x value (g_x = 2.0051) with the hydrogen bond environment. Figure 3 illustrates the ^{2}H Mims ENDOR spectra of ND_2Y_{731}•-$\alpha 2$ compared to ND_2Y_{731}•/R_{411}A-$\alpha 2$. Both spectra contain a broad signal extending over ± 2 MHz arising from the strongly coupled amino deuterons, which is a common feature of ND_2Y• Mims ENDOR spectra.[12, 33] However, we observe that the ^{2}H hf tensor previously assigned to the moderate hydrogen bond between Y_{730} and Y_{731} in ND_2Y_{731}•-$\alpha 2$, which is almost perpendicular to the tyrosine ring plane,[12] is absent in the ND_2Y_{731}•/R_{411}A-$\alpha 2$ spectrum. Therefore, the hydrogen bonding environment of NH_2Y_{731}•/R_{411}A-$\alpha 2$ is distinct from that of the single mutant, consistent with the different side chain conformations observed by HF EPR spectroscopy. Note that almost the complete EPR line of ND_2Y_{731}•/R_{411}A-$\alpha 2$ can be excited at 34 GHz by using very short microwave pulses, and thus hf couplings cannot be missed due to orientation selective effects.

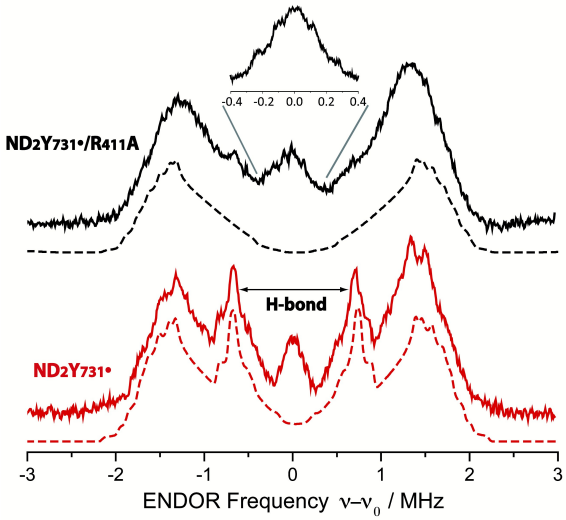

Figure 3. 34-GHz ^{2}H ENDOR spectra of ND_2Y_{731}•/R_{411}A-$\alpha 2$ (solid black line) and ND_2Y_{731}•-$\alpha 2$ (solid red line). Simulations are shown with dashed lines. The hydrogen bond peaks, "H-bond", assigned to a deuteron located between Y_{730}-$\alpha 2$ and ND_2Y_{731}•-$\alpha 2$[12] are not observed in ND_2Y_{731}•/R_{411}A-$\alpha 2$. The inset shows the structured and broad matrix line of ND_2Y_{731}•/R_{411}A-$\alpha 2$. Exp. conditions: Mims ENDOR with $\pi/2$ = 6 ns, τ = 200 ns and 320 ns for the inset, shot repetition time = 15 ms, random RF acquisition[60] with 1 shots/point, acquisition time = 15 – 20 h, T = 70 K. Excitation in the EPR line is set to $B_0 \parallel g_y$. ENDOR spectra are centered at the Larmor frequency of ^{2}H, ν_0 = 7.9 MHz at 1.2 T.

Although no exchangeable moderate hydrogen bonds ($r_{O\text{-}H}$ ~ 1.7 - 2 Å) to ND_2Y_{731}•/R_{411}A-$\alpha 2$ are observed, the ENDOR spectrum of ND_2Y_{731}•/R_{411}A-$\alpha 2$ possesses a broad and structured matrix line, which is associated with weak hf interactions of the radical with distant nuclei[61] (see Figure 3, inset). The structure in this matrix line suggests the existence of weakly coupled deuterons that cannot be resolved from the matrix ones (matrix line). We note that the ENDOR spectrum of ND_2Y_{731}•/R_{411}A-$\alpha 2$ is reminiscent of the one previously observed with the ND_2Y_{356}•-$\beta 2$, also located at the subunit interface and likely surrounded by a defined hydrogen bond network of waters.[12] The similarity between the ENDOR spectra of ND_2Y_{356}•-$\beta 2$ and ND_2Y_{731}•/R_{411}A-$\alpha 2$ suggests a similar origin for the g_x-values in these two mutants, which is distinct from that in ND_2Y_{731}•-$\alpha 2$. As noted above, in the case of ND_2Y_{356}•-$\beta 2$ the g_x-value was also strongly shifted (NH_2Y_{356}•: g_x = 2.0049 vs. free NH_2Y•: g_x = 2.0061[33]). Therefore we propose that the g_x-shift in NH_2Y_{731}•/R_{411}A-$\alpha 2$ as well as in ND_2Y_{356}•-$\beta 2$ arises from weakly coupled hydrogen bonds observed in the 0.3 MHz region of the ENDOR spectrum. The complexity of the **g** tensor interpretation was underlined by our recent DFT calculations, where three distinct models for NH_2Y_{731}•-$\alpha 2$, resulted in similar *g*-shifts.[12] Overall, these data clearly indicate that the molecular orientation of ND_2Y_{731}•/R_{411}A-$\alpha 2$ is different than ND_2Y_{731}•-$\alpha 2$ and is affected by R_{411}A-$\alpha 2$ substitution.

PELDOR gives evidence for a conformational change of ND_2Y_{731}•/R_{411}A-α2. Our previous PELDOR studies[26] have demonstrated that half sites reactivity of *E. coli* RNR allows for the detection of the diagonal inter spin distance between Y_{122}• in one $\alpha\beta$ pair and any radical trapped in the second $\alpha\beta$ pair (Figure 4A).[25, 62] To gain insight into the location of NH_2Y_{731}•/R_{411}A-α2, three sets of PELDOR experiments were recorded using broadband excitation with a high-power Q-band set up at different excitation positions in the EPR line[63-66] (see Figure 4B and S8). The recorded time traces are displayed in Figure 4 and show substantial differences in modulation depth (10 to 50 %), which is typical for orientation selection effects. Trace D1 also shows a higher frequency component that arises from the parallel component of a dipolar pake pattern (Figure S8). For this reason, the background corrected PELDOR time traces from the three sets were summed and the resulting trace was analyzed as shown in Figure 4C and D. Additional comparison of the Fourier-transformed traces (Figure S8) shows that the sum trace leads to an almost complete pake pattern. Distance distribution analysis revealed a clear dominant peak at 35 Å with a distance distribution of Δr = ± 2.7 Å. We note that the error in the peak distance is much less than the distribution and estimated ≤ 0.5 Å. The width of the distance distribution is slightly larger than in previous measurements within the *E. coli* RNR $\alpha 2\beta 2$ complex[25, 26, 62] suggesting more conformational heterogeneity for ND_2Y_{731}•/R_{411}A-α2, consistent with the observed flexibility of this residue. Nevertheless, the results clearly indicate that the mutation of R_{411} induces a conformational change of ND_2Y_{731}• into a new well-defined conformation.

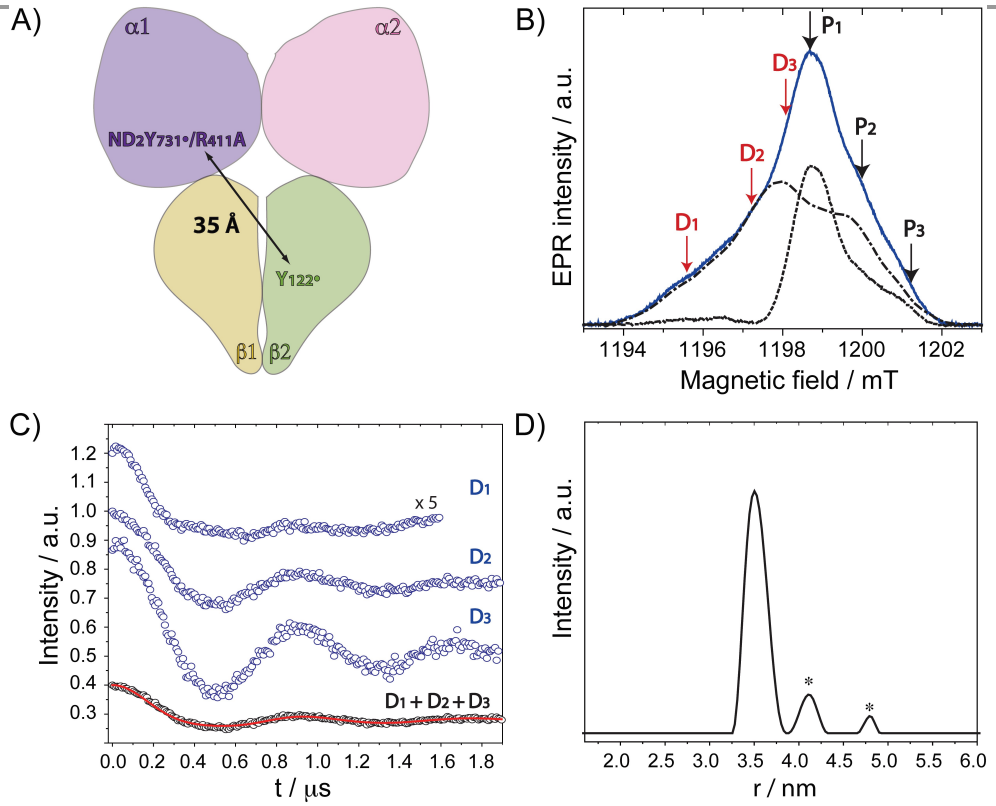

Figure 4. A) Diagonal distance between Y_{122}• in β2 and ND_2Y_{731}•/R_{411}A-α2. **B)** ESE spectrum of ND_2Y_{731}•/R_{411}A-α2 is composed of the Y_{122}•-β2 spectrum (dashed dotted black line) and ND_2Y_{731}•-α2 spectrum (dotted black line). Detect (D) and pump (P) frequency positions for each PELDOR measurement are displayed by red and black arrows, respectively. Exp. conditions (EPR): $\pi/2$ = 6 ns, τ = 280 ns, srt = 120 ms, shots/point = 10, 4 scans, T = 20 K. **C)** Background- and phase-corrected, normalized 34-GHz PELDOR time traces of three experimental setups (D_1, D_2, D_3). The sum of the three traces (D_1+D_2+D_3) is analyzed by DeerAnalysis2015[67] and shown in black with the fitting overlaid in solid red line. Detect/pump π pulse lengths for D_1, D_2 and D_3 were 30 ns/12 ns, 30 ns/12 ns and 20 ns/14 ns, respectively. The frequency separation between detect and pump pulses was 80 MHz for all data sets. **D)** Distance distribution obtained from the analysis in (**C**). Asterisks indicate the artifacts attributed to the analysis procedure

The peak distance 35.0 Å has never been observed before between any radicals formed in the pathway and it is 3 Å shorter than previously measured to ND_2Y_{731}•-α2.[26] This distance might appear rather close to the initial distance (prior to turnover) between the two stable Y_{122}• that is 33.1 Å.[62] To confirm our assignment, we recorded PELDOR experiments at higher temperatures (50 K), where the Y_{122}•-β2 contribution to the refocused echo is filtered and ND_2Y_{731}•-α2 is the only radical species detected (Figure S9). However, Y_{122}•-β2 can still be excited by the pump pulse and contributes to the PELDOR signal. Under these conditions, any distance observed in PELDOR experiments at 50 K is related to Y_{122}• – ND_2Y_{731}• and cannot be associated with the Y_{122}• – Y_{122}• distance, as the latter radical is not detected. The distance distribution analysis of 50 K measurements yielded a peak distance of 35.3 Å with a distribution of Δr ± 2.0 Å, and thus validated our assignment (see Figure S9).

To gain more insight into the conformation o NH_2Y_{731}•/R_{411}A-α2 and the role of R_{411}, we examined the available

X-ray structures of *E. coli* α2s in the region of R_{411}. In the structure of *E. coli* NH_2Y_{730}-α2 (2XO4)[30], Y_{731} is flipped away from NH_2Y_{730} as shown in Fig 5. This altered conformation is compared with a second α in the unit cell in which the Y_{731} is not flipped. To match the 35 Å distance observed by PELDOR spectroscopy, the aromatic ring of NH_2Y_{731} must rotate away from Y_{730} toward the β2 subunit, as observed for Y_{731} with the *E. coli* $Y_{730}NH_2Y$-α2 structure, Fig 5.

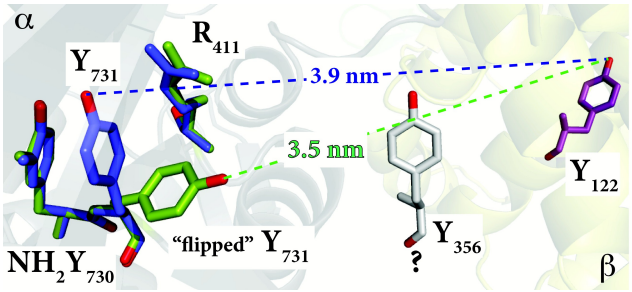

Figure 5. The *E. coli* $Y_{730}NH_2Y$-α2 structure (2XO4)[30] in green shows the reoriented Y_{731} overlaid to the stacked Y_{731} in a different monomer (blue) of the unit cell. The diagonal distance between the "flipped" and non-flipped Y_{731} and Y_{122} are 3.5 nm and 3.9 nm, respectively. These distances, which are between two phenolic oxygens of the tyrosine residues, are based on the alignment with the E. coli $\alpha2\beta2$ docking model. Residue Y_{356} is shown in grey with a "?" because its position is unknown.

This reorientation is also supported by the ENDOR data, which indicate that the stacked conformation between NH_2Y_{731}• and Y_{730} with a shared, perpendicular hydrogen bond is absent in NH_2Y_{731}•/R_{411}A-α2, and that the radical is rather surrounded by weakly coupled hydrogen bonds, likely water molecules at the $\alpha2\beta2$ subunit interface. The exposure of NH_2Y_{731}•/R_{411}A-α2 to the interface and the buffer in this new conformation might be at the origin of the instability of the radical as compared to the single mutant (Table S1).

We have also examined another possible conformation, in which the amino group of NH_2Y_{731}-α2 moves to occupy the vacancy created by mutation of the arginine to alanine. This conformation is displayed in Fig. S10. However, in this case the expected distance between the oxygen of NH_2Y_{731} and Y_{122} exceeds the observed distance by ≥ 2 Å. We note that the "flipped" conformation has not been observed in the single mutant NH_2Y_{731}-α2, or in the double mutant NH_2Y_{731}/Y_{730}F-α2 in which Y_{731} lacks its hydrogen bonding partner,[12] suggesting the importance of R_{411} in stabilizing the stacked conformation. This change between a flipped and non-flipped conformation of this interface Y might play an active role in the PCET process between Y_{731} and Y_{356} in wt RNR, the mechanism of which is still not understood. With the wt enzyme, this conformational change is kinetically masked by physical gating that rate-limits RNR and is too fast to be detected based on the recently measured rate constants for electron transfer (ET) (10^4 to 10^5 s^{-1}) at the interface by photo-RNRs that unmask this gating.[68, 69] Thus the R_{411}A mutation might have fortuitously allowed detection of this movement at the subunit interface.

While the lack of structural information at the subunit interface poses a challenge for a mechanistic understanding of interfacial PCET, the detection of the NH_2Y_{731}• provides us with a spectroscopic probe of this interface. Mutagenesis and site-specific isotopic labeling of interface residues could provide us with additional insight about how this step is controlled. Finally, the mechanism of PCET across the subunit interface observed with the *E. coli* RNR is likely to be conserved in all class I RNRs based on their subunit structures and the conserved weak subunit associations dictated by the C-terminal tail of β2.[70, 71] The pathway for oxidation is conserved between RNRs class Ia, Ib and Ic as is the regulation of the pathway by NDP/effector binding.[72] Thus, while the "details" in the radical transfer mechanism might be different in the individual class I RNRs, general principles will likely emerge from the studies on *E.coli* RNR given all evolutionary conserved features.

Conclusions

This study has revealed that the *E. coli* RNR double mutant NH_2Y_{731}/R_{411}A-α2 unmasks a new conformation of pathway residue 731 in the $\alpha2\beta2$ complex. This is the first experimental evidence for the flexibility of this pathway or any pathway residue in the active enzyme. The results have provided insight about the mechanisms of PCET within α2 as well as through the $\alpha2\beta2$ interface. First, R_{411} appears to play a role in the stabilization of the stacked conformation of Y_{731} and Y_{730} and thus to facilitate collinear PCET within α2 subunit. Second, the new conformation is consistent with Y_{731} pointing toward the subunit interface, the direction of the adjacent pathway residue Y_{356}, located in the flexible C-terminal tail of subunit β2. The flexibility of these two contiguous pathway residues, which have been suggested to communicate during PCET,[69] might be the key to drive the RT chemistry at the subunit interface through water clusters.[6, 7] This opens up a new hypothesis for the PCET mechanism between residues Y_{731}–α2 and Y_{356}–β2, which could involve a gated conformational change of Y_{731}–α2 in wt RNR on a fast time scale, not observable without the R_{411}A mutation. While this hypothesis remains to be proven, the present results will serve as a basis to design new experiments aimed at detecting a possible combined role of Y_{731}–α2 and Y_{356}–β2 in PCET through the subunit surface.

Acknowledgements

We acknowledge Igor Tkach for the help in technical aspects of the HF EPR spectrometers. MK thanks Karin Halbmair for the assistance with PELDOR measurements. We greatly acknowledge financial support for this work from Deutsche Forschungsgemeinschaft (DFG-IRTG 1422 to MK and MB), the Max Planck Society and NIH GM29595 to JS.

References

1. A. Migliore, N. F. Polizzi, M. J. Therien and D. N. Beratan, *Chem. Rev.*, 2014, **114**, 3381-3465.
2. D. N. Beratan, C. Liu, A. Migliore, N. F. Polizzi, S. S. Skourtis, P. Zhang and Y. Zhang, *Acc. Chem. Res.*, 2015, **48**, 474-481.
3. D. R. Weinberg, C. J. Gagliardi, J. F. Hull, C. F. Murphy, C. A. Kent, B. C. Westlake, A. Paul, D. H. Ess, D. G. McCafferty and T. J. Meyer, *Chem. Rev.*, 2012, **112**, 4016-4093.
4. S. Y. Reece, J. M. Hodgkiss, J. Stubbe and D. G. Nocera, *Phil. Trans. R. Soc. B*, 2006, **361**, 1351-1364.

5. S. Y. Reece and D. G. Nocera, *Annu. Rev. Biochem*, 2009, **78**, 673-699.
6. J. Bonin, C. Costentin, C. Louault, M. Robert and J. M. Savéant, *J. Am. Chem. Soc.*, 2011, **133**, 6668-6674.
7. J. M. Savéant, *Annu. Rev. Anal. Chem.*, 2014, **7**, 537-560.
8. R. I. Cukier and D. G. Nocera, *Annu. Rev. Phys. Chem.*, 1998, **49**, 337-369.
9. J. M. Mayer, *Annu. Rev. Phys. Chem.*, 2004, **55**, 363-390.
10. A. Jordan and P. Reichard, *Annu. Rev. Biochem*, 1998, **67**, 71-98.
11. J. Stubbe and W. A. Van Der Donk, *Chem. Rev.*, 1998, **98**, 705-762.
12. T. U. Nick, W. Lee, S. Koßmann, F. Neese, J. Stubbe and M. Bennati, *J. Am. Chem. Soc.*, 2015, **137**, 289-298.
13. L. Thelander, *J. Biol. Chem.*, 1973, **248**, 4591-4601.
14. E. C. Minnihan, D. G. Nocera and J. Stubbe, *Acc. Chem. Res.*, 2013, **46**, 2524-2535.
15. N. C. Brown and P. Reichard, *J. Mol. Biol.*, 1969, **46**, 25-38.
16. N. C. Brown and P. Reichard, *J. Mol. Biol.*, 1969, **46**, 39-55.
17. A. Hofer, M. Crona, D. T. Logan and B. M. Sjöberg, *Crit. Rev. Biochem. Mol. Biol.*, 2012, **47**, 50-63.
18. J. A. Stubbe, *J. Biol. Chem.*, 1990, **265**, 5329-5332.
19. M. Eriksson, U. Uhlin, S. Ramaswamy, M. Ekberg, K. Regnström, B. M. Sjöberg and H. Eklund, *Structure*, 1997, **5**, 1077-1092.
20. A. Ehrenberg and P. Reichard, *J. Biol. Chem.*, 1972, **247**, 3485-3488.
21. B. M. Sjoberg, P. Reichard, A. Graslund and A. Ehrenberg, *J. Biol. Chem.*, 1978, **253**, 6863-6865.
22. P. Nordlund, B. M. Sjöberg and H. Eklund, *Nature*, 1990, **345**, 593-598.
23. U. Uhlin and H. Eklund, *Nature*, 1994, **370**, 533-539.
24. J. A. Stubbe, D. G. Nocera, C. S. Yee and M. C. Y. Chang, *Chem. Rev.*, 2003, **103**, 2167-2201.
25. M. Bennati, J. H. Robblee, V. Mugnaini, J. Stubbe, J. H. Freed and P. Borbat, *J. Am. Chem. Soc.*, 2005, **127**, 15014-15015.
26. M. R. Seyedsayamdost, C. T. Y. Chan, V. Mugnaini, J. Stubbe and M. Bennati, *J. Am. Chem. Soc.*, 2007, **129**, 15748-15749.
27. N. Ando, E. J. Brignole, C. M. Zimanyi, M. A. Funk, K. Yokoyama, F. J. Asturias, J. Stubbe and C. L. Drennan, *Proc. Natl. Acad. Sci. U. S. A.*, 2011, **108**, 21046-21051.
28. E. C. Minnihan, N. Ando, E. J. Brignole, L. Olshansky, J. Chittuluru, F. J. Asturias, C. L. Drennan, D. G. Nocera and J. Stubbe, *Proc. Natl. Acad. Sci. U. S. A.*, 2013, **110**, 3835-3840.
29. J. Ge, G. Yu, M. A. Ator and J. Stubbe, *Biochemistry*, 2003, **42**, 10071-10083.
30. E. C. Minnihan, M. R. Seyedsayamdost, U. Uhlin and J. Stubbe, *J. Am. Chem. Soc.*, 2011, **133**, 9430-9440.
31. K. R. Ravichandran, E. C. Minnihan, Y. Wei, D. G. Nocera and J. Stubbe, *J. Am. Chem. Soc.*, 2015, **137**, 14387-14395.
32. M. R. Seyedsayamdost, J. Xie, C. T. Y. Chan, P. G. Schultz and J. Stubbe, *J. Am. Chem. Soc.*, 2007, **129**, 15060-15071.
33. T. Argirević, C. Riplinger, J. Stubbe, F. Neese and M. Bennati, *J. Am. Chem. Soc.*, 2012, **134**, 17661-17670.
34. M. R. Seyedsayamdost, T. Argirević, E. C. Minnihan, J. Stubbe and M. Bennati, *J. Am. Chem. Soc.*, 2009, **131**, 15729-15738.
35. B. Wörsdörfer, D. A. Conner, K. Yokoyama, J. Livada, M. Seyedsayamdost, W. Jiang, A. Silakov, J. Stubbe, J. M. Bollinger and C. Krebs, *J. Am. Chem. Soc.*, 2013, **135**, 8585-8593.
36. K. Yokoyama, U. Uhlin and J. Stubbe, *J. Am. Chem. Soc.*, 2010, **132**, 8385-8397.
37. S. P. Salowe, M. A. Ator and J. Stubbe, *Biochemistry*, 1987, **26**, 3408-3416.
38. S. P. Salowe and J. Stubbe, *J. Bacteriol.*, 1986, **165**, 363-366.
39. P. T. Chivers, K. E. Prehoda, B. F. Volkman, B. M. Kim, J. L. Markley and R. T. Raines, *Biochemistry*, 1997, **36**, 14985-14991.
40. M. Russel and P. Model, *J. Bacteriol.*, 1985, **163**, 238-242.
41. J. R. Steeper and C. D. Steuart, *Anal. Biochem.*, 1970, **34**, 123-130.
42. S. Climent, B. M. Sjöberg and C. Y. Huang, *Biochemistry*, 1991, **30**, 5164-5171.
43. A. Savitzky and M. J. E. Golay, *Anal. Chem.*, 1964, **36**, 1627-1639.
44. S. Stoll and A. Schweiger, *J. Magn. Reson.*, 2006, **178**, 42-55.
45. F. Neese, *Wiley Interdisciplinary Reviews: Computational Molecular Science*, 2012, **2**, 73-78.
46. A. D. Becke, *Phys. Rev. A*, 1988, **38**, 3098-3100.
47. A. D. Becke, *J. Chem. Phys.*, 1993, **98**, 5648-5652.
48. C. Lee, W. Yang and R. G. Parr, *Physical Review B*, 1988, **37**, 785-789.
49. A. Schäfer, C. Huber and R. Ahlrichs, *J. Chem. Phys.*, 1994, **100**, 5829-5835.
50. F. Weigend and R. Ahlrichs, *PCCP*, 2005, **7**, 3297-3305.
51. A. Klamt and G. Schüürmann, *J. Chem. Soc., Perkin Trans. 2*, 1993, 799-805.
52. S. Grimme, J. Antony, S. Ehrlich and H. Krieg, *J. Chem. Phys.*, 2010, **132**.
53. S. Grimme, S. Ehrlich and L. Goerigk, *J. Comput. Chem.*, 2011, **32**, 1456-1465.
54. F. Neese, F. Wennmohs, A. Hansen and U. Becker, *Chem. Phys.*, 2009, **356**, 98-109.
55. S. Kossmann, B. Kirchner and F. Neese, *Mol. Phys.*, 2007, **105**, 2049-2071.
56. F. Neese, in *Multifrequency Electron Paramagnetic Resonance*, ed. S. K. Misra, Wiley-VCH Verlag GmbH & Co. KGaA, 2011, ch. 6, pp. 295-326.
57. S. Un, M. Atta, M. Fontecave and A. W. Rutherford, *J. Am. Chem. Soc.*, 1995, **117**, 10713-10719.
58. H. M. McConnell, *J. Chem. Phys.*, 1956, **24**, 764-766.
59. R. W. Fessenden and R. H. Schuler, *J. Chem. Phys.*, 1963, **39**, 2147-2195.
60. B. Epel, D. Arieli, D. Baute and D. Goldfarb, *J. Magn. Reson.*, 2003, **164**, 78-83.
61. A. V. Astashkin and A. Kawamori, *J. Magn. Reson.*, 1998, **135**, 406-417.
62. M. Bennati, A. Weber, J. Antonic, D. L. Perlstein, J. Robblee and J. Stubbe, *J. Am. Chem. Soc.*, 2003, **125**, 14988-14989.
63. V. P. Denysenkov, T. F. Prisner, J. Stubbe and M. Bennati, *Proc. Natl. Acad. Sci. U. S. A.*, 2006, **103**, 13386-13390.
64. A. D. Milov, A. G. Maryasov and Y. D. Tsvetkov, *Appl. Magn. Reson.*, 1998, **15**, 107-143.
65. Y. Polyhach, A. Godt, C. Bauer and G. Jeschke, *J. Magn Reson.*, 2007, **185**, 118-129.
66. G. Sicoli, T. Argirević, J. Stubbe, I. Tkach and M. Bennati, *Appl. Magn. Reson.*, 2010, **37**, 539-548.

67. G. Jeschke, V. Chechik, P. Ionita, A. Godt, H. Zimmermann, J. Banham, C. R. Timmel, D. Hilger and H. Jung, *Appl. Magn. Reson.*, 2006, **30**, 473-498.
68. L. Olshansky, A. A. Pizano, Y. Wei, J. Stubbe and D. G. Nocera, *J. Am. Chem. Soc.*, 2014, **136**, 16210-16216.
69. D. Y. Song, A. A. Pizano, P. G. Holder, J. Stubbe and D. G. Nocera, *Chemical Science*, 2015, **6**, 4519-4524.
70. M. Kolberg, K. R. Strand, P. Graff and K. K. Andersson, *Biochim. Biophys. Acta*, 2004, **1699**, 1-34.
71. Y. Zhang, X. An, J. Stubbe and M. Huang, *J. Biol. Chem.*, 2013, **288**, 13951-13959.
72. P. Nordlund and P. Reichard, *Annu. Rev. Biochem*, 2006, **75**, 681-706.